Partial crystallization and melting of an Se sublattice in the superionic conductor Ag_2Se: a molecular dynamics study

1993 J. Phys.: Condens. Matter 5 3405

(http://iopscience.iop.org/0953-8984/5/21/003)

J. Phys.: Condens. Matter 5 (1993) 3405–3416. Printed in the UK

Partial crystallization and melting of an Se sublattice in the superionic conductor Ag_2Se: a molecular dynamics study

F Shimojo† and H Okazaki‡

† Graduate School of Science and Technology, Niigata University, Niigata 950-21, Japan
‡ College of General Education, Niigata University, Niigata 950-21, Japan

Received 1 September 1992, in final form 8 February 1993

Abstract. The partial crystallization and melting of the Se sublattice in the superionic conductor Ag_2Se are investigated by means of a constant-pressure and constant-temperature molecular dynamics simulation. The effective interionic potential of Rino *et al* is used. The transition temperature is estimated to be about 1000 K, which is reasonable in comparison with the actual transition temperature, 1170 K. The atomic structures of the Se sublattice in the crystallization and melting processes are analysed by the method of the Voronoi polyhedron. The defect formation process before melting is studied in detail from a microscopic point of view. It is shown that, in the superionic phase, the repulsive force acting on an Se ion from its neighbouring Ag ions behaves as the restoring force maintaining the Se BCC sublattice, and that an opportunity to create the defect is given when the restoring force weakens.

1. Introduction

In order to understand the nature of superionic conductors it is necessary to study not only the superionic (α) phase, but also the phase changes between the non-superionic (β) $\leftrightarrow$ α phases and the $\alpha \leftrightarrow$ molten phases. As the α phase is structurally in a highly disordered state, it is difficult to discuss the phase changes by purely theoretical methods, and instead computer simulation is a powerful method to treat them.

Molecular dynamics (MD) simulation is a suitable method for studying disordered systems such as superionic conductors. Since the pioneering work by Rahman [1] for CaF_2, the MD method has been applied to several kinds of these substances. Gillan and co-workers have energetically applied the MD simulations to fluorite-type superionic conductors, such as $SrCl_2$ [2, 3], PbF_2 [4] and CaF_2 [5, 6], in order to investigate the dynamical properties of ions. They have shown that, for $SrCl_2$ and PbF_2, the spatial distribution of anions in the disordered state is in agreement with the results of neutron diffraction measurements [7], and that anion migrations preferentially occur in the [100] direction. For CaF_2, Gillan first observed correlated motion of anions, and has calculated the partial dynamical structure factors which should be compared with neutron scattering experiments. Wolf *et al* [8] have studied structure and transport properties of the two-dimensional superionic conductor Li_3N. These works are important in the sense that the diffusion mechanism of mobile ions has been made clear.

Since Andersen [9] proposed an MD method for a constant-enthalpy and constant-pressure (H, P, N) ensemble, we have been able to study the phase transition phenomena by a computer simulation. For superionic conductors, Parrinello *et al* [10] applied the MD method to AgI and have shown that the $\alpha \leftrightarrow \beta$ phase transition occurs. Tallon [11] succeeded in reproducing the P–T phase diagram of AgI established experimentally. Ray

0953-8984/93/213405+12$07.50

and Vashishta [12] also studied the $\alpha \leftrightarrow \beta$ phase transition in Ag_2S whose α phase structure is similar to α-AgI. Recently, we have simulated the $\alpha \leftrightarrow \beta$ phase transition in Ag_2Se [13] with the effective pair-wise potential of Rino *et al* [14] and have shown that the β phase structure is very similar to that determined experimentally [15] though the former has a slightly higher symmetry than the latter. Until the present time, however, no study on the crystallization or melting in the superionic conductors has been reported, apart from the work on Lennard-Jones systems such as an inert Ar liquid [16–18], soft-core repulsion systems as ideal neutral particles [19–23] and Coulomb and soft-core systems such as alkali halides [24]. The crystallization and melting in Ag_2Se are interesting problems in the sense that the structural transformations of the Se sublattice have to be realized with cations remaining in disorder.

The success of the computer simulation strongly depends on the model potential for the system considered. For Ag_2Se, Rino *et al* [14] found a suitable potential and have succeeded in reproducing the structural and dynamical properties of the superionic and molten states by using a constant-volume MD simulation. In this paper, we report the partial crystallization and melting processes of the Se sublattice in Ag_2Se by a constant-pressure and constant-temperature (N, P, T) MD method using the potential of Rino *et al* [14].

2. Method of MD calculations

The MD simulations are performed using the (N, P, T) technique. To retain the MD cell at a constant temperature, the method proposed by Nosé [25–27] is used. The temperature is controlled by introducing a variable s which acts as the heat reservoir to the cell [25]. To perform a constant-pressure calculation, the algorithm proposed by Andersen [9] is used. For a cube of volume V, the edge length of the MD cell, $L = V^{1/3}$, is introduced as a dynamical variable and each of the particle positions $\boldsymbol{r}_i$ is normalized to be $\boldsymbol{q}_i = \boldsymbol{r}_i/L$ whose components are limited to ~ 0–1. Then the equations of motion for ions and variables are given as follows [18, 27]

$$\ddot{\boldsymbol{q}}_i = -\frac{1}{m_i L}\frac{\partial \Phi_N}{\partial \boldsymbol{r}_i} - \left(\frac{\dot{s}}{s} + 2\frac{\dot{L}}{L}\right)\dot{\boldsymbol{q}}_i \qquad (i = 1, \ldots, N) \tag{1}$$

$$\ddot{s} = \frac{s}{Q}\left(\sum_i m_i L^2 \dot{\boldsymbol{q}}_i^2 - 3Nk_B T\right) + \frac{\dot{s}^2}{s} \tag{2}$$

$$\ddot{L} = \frac{s^2}{wL^2}\left\{\left(\frac{1}{3V}\sum_i m_i L^2 \dot{\boldsymbol{q}}_i^2 - \frac{\partial \Phi_N}{\partial V}\right) - P\right\} + \frac{\dot{s}}{s}\dot{L} - 2\frac{\dot{L}^2}{L} \tag{3}$$

where Φ_N is the potential energy of the N-particle system, m_i the mass of the ith particle, k_B the Boltzmann constant, T the temperature and P is the external pressure applied to the cell. The overdots denote the time derivatives. Q and w are parameters with dimensions of energy(time)^2 and mass/(length)^4 respectively. These parameters determine the time scale of the volume and temperature fluctuations of the MD cell, but do not give any effect in the equilibrium state.

The effective interionic potential proposed by Rino *et al* is composed of three interactions: Coulomb interaction, core repulsion and charge–dipole interaction. The

potential has the form:

$$V_{AgAg}(r) = 0.2025/r + 0.2408/r^{11}$$
$$V_{AgSe}(r) = -0.405/r + 86.6614/r^9 - 0.7088(\exp(-r/4.43)/r^4) \quad (4)$$
$$V_{SeSe}(r) = 0.81/r + 220.1905/r^7 - 5.67(\exp(-r/4.43)/r^4)$$

where r is the distance between ions. Energy units are given by e^2 Å^{-1} = 14.40 eV. The electronic polarizability for an Ag ion is much smaller than that for an Se ion, therefore it is taken to be zero so that there is no term related to it in V_{AgAg} [14].

The calculations are carried out for a system of 384 (256 Ag^+ + 128 Se^{2-}) ions in a cubic form. The equations of motion are solved via Gear's predictor–corrector algorithm [28] with time step $\Delta t = 6.0 \times 10^{-15}$ s. For Q and w, we choose ~ 26–40 kJ mol^{-1} ps^{-2} and 1.8×10^{-3} g mol^{-1} Å^{-4} respectively. The external pressure is taken as $P = 2.0$ GPa, which was employed in the study of the α–β phase transition in Ag_2Se [13]. The usual periodic boundary conditions are imposed and the Ewald sum method is used for evaluating the long-range Coulomb interactions. Other terms in the potential are calculated by direct summation within a cut-off length of ~ 7.5 Å and by integration beyond the cut-off length using the continuum approximation.

The calculation begins at the state where Se ions sit on the BCC lattice points and Ag ions on 12(d) sites, in an appropriate way, at 1400 K. After a few thousand time steps, the anion BCC sublattice is destroyed and the system changes into a molten state. By simulation in the molten state for 25 000 time steps, it is confirmed that several properties, such as partial distribution functions, three-body bond-angle distributions and diffusivity, are in good agreement with those obtained by Rino *et al* [14]. Then the temperature is lowered to 1200 K in decrements of 100 K and below 1200 K in decrements of 50 K. After partial crystallization of the Se sublattice at 800 K, the system is heated up in increments of 50 K until the molten state reappears. At each temperature, the calculation is usually performed for 25 000 time steps. The initial 10 000 time steps after a change of temperature are regarded as the aging of the system, and physical quantities are obtained by taking the time average after the aging.

In order to examine the crystallization, melting and glass transition processes, the method of the Voronoi polyhedra [29, 30] has been used by several authors [18–20, 22, 31, 32]. We also utilize the Voronoi polyhedra analysis for studying the microscopic behaviour of the partial crystallization and melting of the Se sublattice in Ag_2Se. The Voronoi polyhedron is defined as follows. We take up an ion i and all other ions j and make planes perpendicular to r_i–r_j through its midpoint, where r_i and r_j are the position vectors of ions i and j, respectively. These planes make polyhedra enclosing the ion i inside. The smallest polyhedron among them is called the Voronoi polyhedron of the ion i. Thus, if ions are arranged in an ordered way, the Voronoi polyhedron is just the same as the Wigner–Seitz cell. For ions arranged in a disordered way, the Voronoi polyhedron is different. Each Voronoi polyhedron is characterized by a set of integers $(n_3, n_4, n_5, \ldots)$ and the total number of faces F, where n_k is the number of k-edged faces and $F = \sum_k n_k$. The perfect BCC crystal consists of only one kind of Voronoi polyhedron described by (0608). By an elementary process (figure 1) the (0608) polyhedron turns into three polyhedra, (0446), (15152) and (15162), which are called the (0608)-family polyhedra hereafter. For the evaluation of the Voronoi polyhedra, we use the time-averaged positions of Se ions over 50 time steps in both the α and molten phases in order to eliminate the effect of thermal vibration.

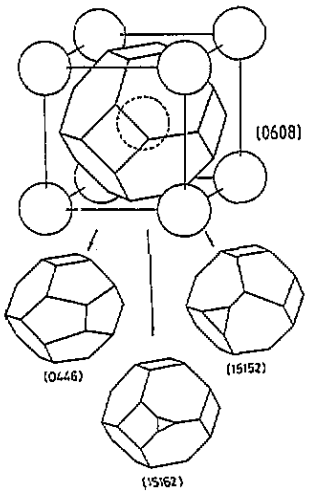

Figure 1. Stereographic projections of the (0608) polyhedron and (0608)-family, i.e. (0446), (15152) and (15162), polyhedra. Circles denote Se ions forming the BCC unit cell.

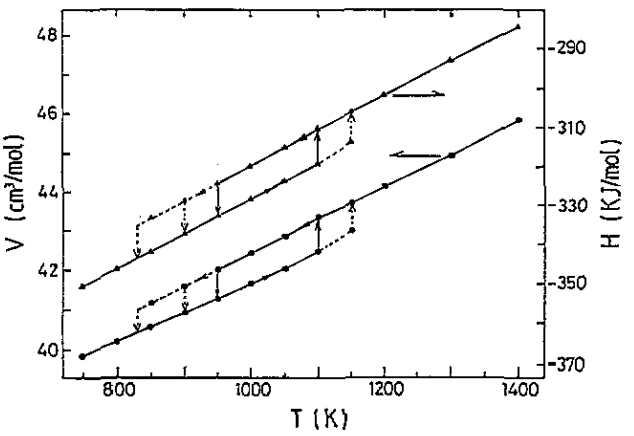

Figure 2. Temperature dependences of molar volume (circles) and enthalpy (triangles).

3. Results and discussion

3.1. Transition temperature and self-diffusion coefficient

The temperature dependences of molar volume and enthalpy are shown in figure 2. The partial crystallization of the Se sublattice is observed between 800 and 850 K at a cooling rate of 50 K/25 000 time steps. When the calculations continue after the 25 000 time steps at 900 and 950 K, crystallization takes place at about 30 000 and 50 000 time steps respectively. However, at 1000 K, crystallization does not take place for the calculation of 120 000 time steps. On the other hand, by heating up the α phase at a rate of 50 K/25 000 time steps, the system melts again at 1150 K. When the calculation is performed at 1100 K, the melting is observed at about 85 000 time steps. However, at 1050 K, the system keeps the α phase over the calculation of 120 000 time steps. Thus, there exists a large hysteresis between the crystallization and melting points at a rate of 50 K/25 000 time steps and the longer the calculation, the narrower the hysteresis range. Then, the transition temperature is estimated to be about 1000 K, which is reasonable in comparison with the experimental value, 1170 K.

The latent heat and volume change at the transitions, and the expansion coefficients in the α and molten phases, are listed in table 1 together with the values at the $\alpha \rightarrow \beta$ phase transition [13]. The latent heat at melting is larger than that at the $\alpha \rightarrow \beta$ phase transition. This implies that melting of the Se sublattice needs a larger energy than the partial melting of the Ag sublattice accompanying the structural transformation of the Se sublattice. This is reasonable since the Coulomb energy felt by an Se ion is large because it is divalent and its sublattice has a high melting temperature. No experimental value of the latent heat at melting in Ag_2Se has been reported, but the above relation is satisfied in Ag_2S [34], in the family of Ag_2Se.

Table 1.

Latent heat ΔH		
	($\alpha \rightarrow$ molten)	8.2 kJ mol^{-1}
	(molten $\rightarrow \alpha$)	−8.5 kJ mol^{-1}
	cf ($\alpha \rightarrow \beta$)[a]	−3.0 kJ mol^{-1}
Volume change ΔV		
	($\alpha \rightarrow$ molten)	0.80 cm^3 mol^{-1} (1.9%)
	(molten $\rightarrow \alpha$)	−0.75 cm^3 mol^{-1} (−1.8%)
	cf ($\alpha \rightarrow \beta$)[a]	−1.24 cm^3 mol^{-1} (−3.0%)
Expansion coefficient		
α phase	(750 K–950 K)	1.8×10^{-4} K^{-1}
	cf (500 K–590 K)[a]	1.5×10^{-4} K^{-1}
Molten phase	(1150 K–1500 K)	1.9×10^{-4} K^{-1}

[a] [13].

Even after the crystallization of the Se sublattice, Ag ions remain in the disordered state. The self-diffusion coefficient for Ag ions, D_{Ag}, is estimated from the relation of the mean square displacement against time, and its temperature dependence is shown by filled circles in figure 3. D_{Ag} for the α and molten phases are expressed in the Arrhenius form as

$$D_{Ag}^{\alpha} = 3.0 \times 10^{-4} e^{-0.14\ eV/k_B T}\ cm^2\ s^{-1} \tag{5}$$

and

$$D_{Ag}^{m} = 7.0 \times 10^{-4} e^{-0.20\ eV/k_B T}\ cm^2\ s^{-1} \tag{6}$$

respectively. D_{Ag}^{α} is in good agreement with the result obtained from the experiment [33] between 420 and 570 K by one of the present authors. The anion self-diffusion coefficient in the molten phase is shown by open circles in figure 3, and is given by

$$D_{Se}^{m} = 3.6 \times 10^{-4} e^{-0.26\ eV/k_B T}\ cm^2\ s^{-1}. \tag{7}$$

The activation energy of D_{Ag}^{m} is smaller than that of D_{Se}^{m} while values of D_{Ag}^{m} are always larger than those of D_{Se}^{m}. This may be understood by the fact that the anion radius is larger than that of the cation and the anion charge is twice the cation charge, resulting in an increase of potential felt by the anion.

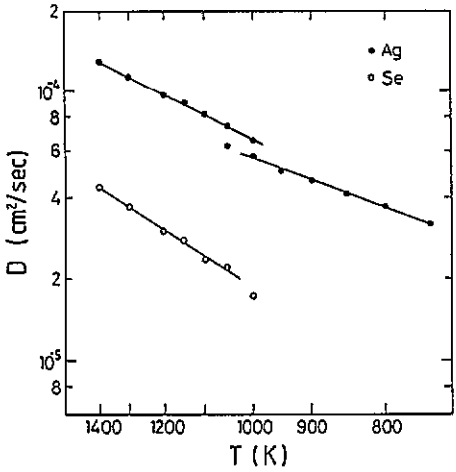

Figure 3. Temperature dependences of the self-diffusion coefficients for Ag ions (filled circles) and Se ions (open circles).

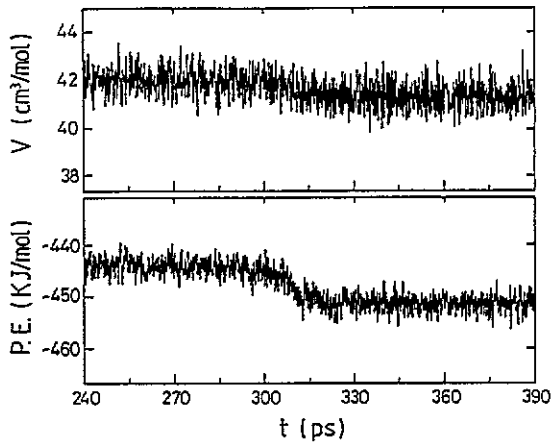

Figure 4. Changes of molar volume and potential energy for the crystallization process as a function of time. Time is measured from the instant when the temperature is switched to 950 K.

3.2. Partial crystallization of anions

Figure 4 shows the changes in volume and potential energy as functions of time at 950 K for the crystallization process. The time is measured from the instant when the temperature is switched to 950 K from 1000 K. Until about 300 ps (50 000 time steps) the system is in the molten state. Abrupt decreases in these quantities are observed at ~ 300–320 ps, and the system changes into a different state. In order to see how the crystallization of the Se sublattice occurs, we study the Voronoi polyhedra formed by Se ions. As the Se sublattice forms the BCC lattice in the α phase, the corresponding Voronoi polyhedron being (0608), we investigate the time dependence of the percentage of (0608) polyhedra to total Voronoi polyhedra. The result is shown in figure 5, in which open and filled circles show the percentages of the (0608), and (0608) plus (0608)-family polyhedra, respectively. Each circle is the average value over 1000 time steps, namely, over 20 configurations where each configuration is formed by the time average positions of Se ions over 50 time steps. In the molten state region, the percentages are almost zero and they begin to increase suddenly at about 300 ps. Then they reach constant values in a short period, which indicates that the Se sublattice crystallizes to the BCC structure. The fact that their percentages are smaller than 100% is caused by the large amplitudes of lattice vibrations of Se ions from their equilibrium positions at high temperature.

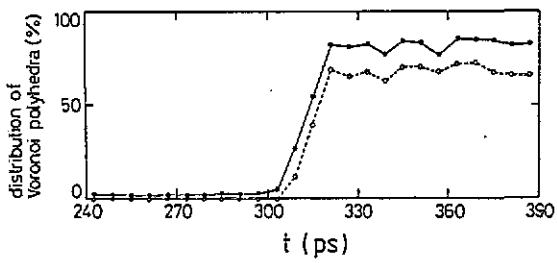

Figure 5. Time evolution of percentages of (0608) polyhedra (open circles) and of (0608)-family polyhedra including (0608) (filled circles) for the crystallization process.

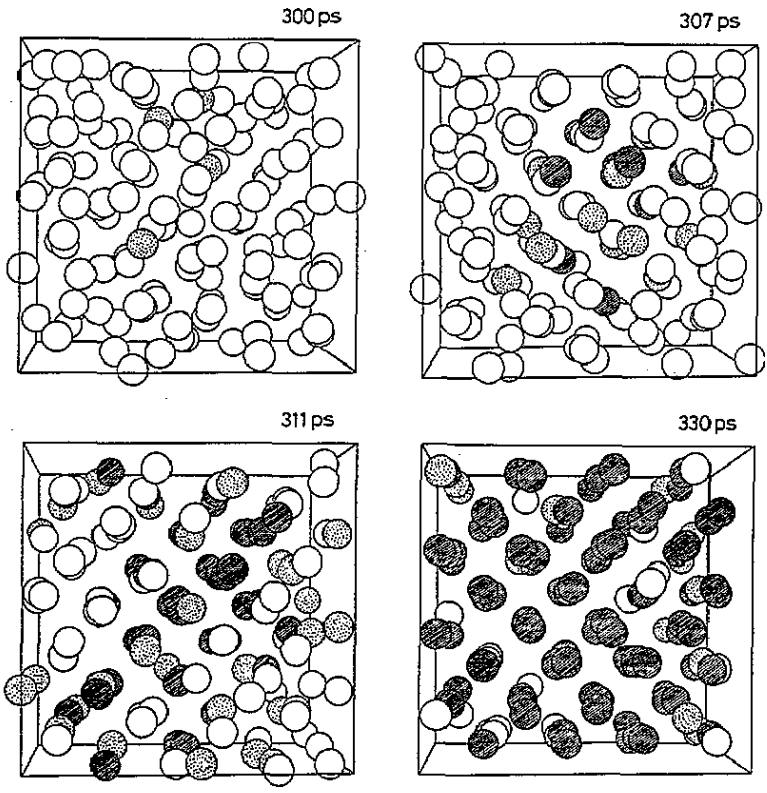

Figure 6. *Arrangements of Se ions in the* MD *cell. Circles with oblique lines denote Se* ions having a (0608) polyhedron and circles with dots denote Se ions having a (0608)-family polyhedron. Times in the figures correspond to the abscissas of figures 4 and 5.

This crystallization can be directly confirmed by observing the process by which the Se BCC arrangement is formed. Figure 6 shows a three-dimensional bird's-eye view of the arrangement of Se ions in the MD cell at 300, 307, 311 and 330 ps. In these figures, the Se ions with oblique lines form the (0608) polyhedra and the Se ions with dots form the (0608)-family polyhedra. At 300 ps, the system is in a molten state and there is no (0608) Se ion, only a few (0608)-family Se ions. At 307 ps, several (0608) Se ions appear with a comparable number of (0608)-family Se ions. We see that the lines of Se arrangement begin to grow. At 311 ps, it is recognized that both (0608) and its family ions increase and the lines of Se arrangement become clearer. Finally, at 330 ps, most Se ions are (0608) ions, and the lines of Se arrangement are clearly established, indicating that the Se sublattice crystallizes to the BCC lattice.

3.3. Melting of anions

The changes in volume and potential energy for the melting process at 1100 K are shown in figure 7. We see that the melting of the Se sublattice takes place at about 510 ps (85 000 time steps). Figure 8 shows the time dependences of distributions of the (0608) and (0608) plus (0608)-family polyhedra. Before 510 ps, the Se sublattice is basically the BCC structure, but the percentages of the (0608) and (0608)-family polyhedra are rather smaller than in

figure 5. This means that the Voronoi polyhedra are more distorted by thermal vibrations of Se ions at higher temperature.

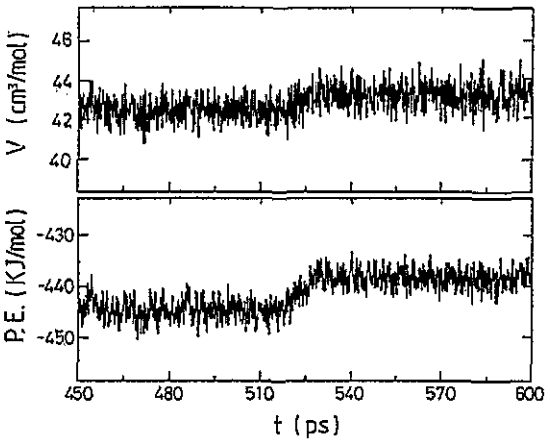

Figure 7. Changes of molar volume and potential energy for the melting process as a function of time. Time is measured from the instant when the temperature is switched to 1100 K.

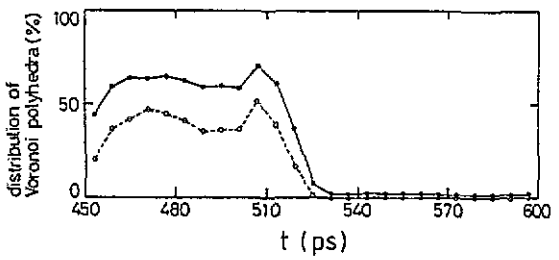

Figure 8. Time evolution of percentages of (0608) polyhedra (open circles) and of (0608)-family polyhedra including (0608) (filled circles) for the melting process.

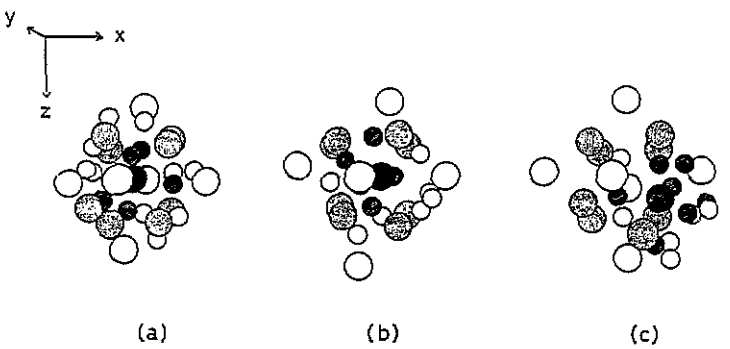

Figure 9. Arrangements of Se and Ag ions around an Se ion (large filled circle). Large circles with dots are the first-neighbour Se ions and large open circles are the second-neighbour Se ions. Small circles show Ag ions within 5.0 Å of the Se ion, those with oblique lines show Ag ions within 3.5 Å.

Before the melting, we observe the formation of anion Frenkel defects. A typical example of the defect formation is shown in figure 9. Figure 9(*a*) shows the arrangement of Se and Ag ions around the Se ion marked with the large filled circle at an instant at 1050 K, where large dotted circles are its first-neighbouring Se ions and large open circles are its second-neighbouring Se ions. We see that Se ions form the BCC structure. Small circles show Ag ions within 5.0 Å of the Se ion; those with oblique lines show Ag ions within 3.5 Å, which is the position of the first minimum in the Ag–Se pair distribution function. After 100 time steps from the instant in figure 9(*a*), the arrangement of Ag and Se ions is changed as shown in figure 9(*b*), from which it can be seen that the Se ion moves towards the right and the four Se ions with dots to the right of it are expanded so as to help it move to the centre of them, i.e. the interstitial position of the BCC lattice. Furthermore, it is recognized that the Ag distribution within 3.5 Å of the Se ion is markedly deviated to the left-hand side of it, which also forces the Se ion to move towards the right. Thus, in the formation process of the Se defect, a great alteration in the local density of Ag ions takes place and this is accompanied by a similar effect in the local density of Se ions. When more than 100 time steps have passed, the metastable interstitial position of the BCC lattice as shown in figure 9(*c*) is reached.

In figure 10(*a*), the migration of the solid Se ion towards the right described above is shown by a dotted curve as a function of time. The x axis is defined from the body centre lattice point initially occupied by the Se ion to the interstitial point to which it travels. In order to study the microscopic mechanism of the defect formation, we examine the x component of the total force, F_x, acting on the Se ion, which is shown as a full curve in the figure. We see that, before the migration, the Se ion makes a vibrational motion around the normal site and F_x acts as the restoring force, i.e. its direction is opposite to the displacement x and its amplitude is proportional to x. For a short period just before the Se ion begins to migrate, the amplitude of F_x is relatively small and the restoring work of F_x weakens. Once the migration begins it continues until the Se ion arrives at the interstitial site even though a periodically changing force acts on it. The vertical arrows in the figure indicate the times corresponding to the figures 9(*a*), (*b*) and (*c*), respectively.

Next, we divide F_x into three components, F_x^C, $F_x^S(\mathrm{Ag})$ and $F_x^S(\mathrm{Se})$, and plot them in figure 10(*b*), where the broken curve shows F_x^C, the Coulomb force, and the fine and bold curves show $F_x^S(\mathrm{Ag})$ and $F_x^S(\mathrm{Se})$, short-range forces from surrounding Ag and Se ions, respectively. $F_x^S(\mathrm{Ag})$ and $F_x^S(\mathrm{Se})$ are composed of two terms of core repulsion and charge–dipole interaction. By comparing figures 10(*a*) with (*b*), it is seen that the main contribution to F_x is from $F_x^S(\mathrm{Ag})$ and it is slightly modulated by F_x^C fluctuating slowly. The contribution of $F_x^S(\mathrm{Se})$ to F_x is small, which is reasonable as direct contact of the same kind of ion is illegal in ionic crystals. Although the main part of the restoring force is due to $F_x^S(\mathrm{Ag})$ as stated above, the repulsive part in it is more important, as the contribution of the charge–dipole interaction to $F_x^S(\mathrm{Ag})$ is about 30% at an Ag–Se average distance 2.8 Å.

Figure 10(*c*) shows the change in the distortion parameter, w_i, of the Voronoi polyhedron of the Se ion, which is defined as follows [18]:

$$w_i = \frac{S_i/4\pi}{(V_i/(4\pi/3))^{2/3}} \tag{8}$$

where S_i and V_i denote the surface area and the volume of the ith Voronoi polyhedron respectively. w_i is unity if a Voronoi polyhedron is a sphere and it has a value 1.099 for the ideal (0608) polyhedron. With the defect formation, the value of w_i increases abruptly to a maximum at the completion of the defect and reduces to the initial value. This implies that Se ions around the defect Se ion are rearranged. When we further follow the motion

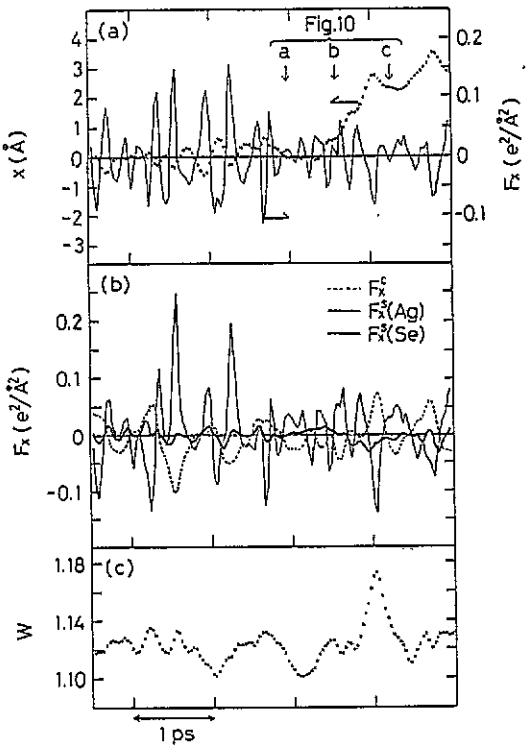

Figure 10. (*a*) Time dependences of the x coordinate of the Se ion in figure 9 (dotted curve), and the x component of the total force, F_x, acting on it (full curve). (*b*) Time dependences of Coulomb force, F_x^C (broken curve), and short-range forces from surrounding Ag and Se ions, F_x^S(Ag) (fine curve) and F_x^S(Se) (bold curve) respectively, where $F_x = F_x^C + F_x^S(\mathrm{Ag}) + F_x^S(\mathrm{Se})$. (*c*) Time dependence of the distortion parameter, w_i, of the Voronoi polyhedron of the Se ion.

of the Se ion, we find that it migrates to a new normal site after staying in the interstitial site for a while, resulting in Se diffusion in the α phase.

As mentioned above, the distribution of Ag ions around Se ions is important to create the Se defect, so we calculate the number of Ag ions around each Se ion. By connecting all contiguous pairs of Se ions a network is obtained, where the contiguous pair is defined as a pair whose Voronoi polyhedra have a face in common. A tetrahedron formed of a set of four Se ions in this network is called the Delaunay tetrahedron. We define an Ag ion neighbouring an Se ion as an Ag ion within one of the Delaunay tetrahedra around the Se ion. In figure 11, the histograms of the number of neighbour Ag ions in the superionic (fine lines with shading at 950 K) and molten (bold lines at 1200 K) states are shown. The average number is eight for both states, but there exists a clear difference in the standard deviation of the distribution, which is defined as $\delta N = \sqrt{\langle (N - \bar{N})^2 \rangle}$ with $\bar{N} = 8$. The temperature dependence of δN is shown in figure 12. We see that it decreases rapidly towards the melting point.

For studying the melting phenomena of a Coulomb system similar to the present system, Amini *et al* [24] applied an MD method to a Coulomb and soft-core system acting as an alkali halide. They did not use the periodic boundary condition for the system, so their work is concerned with the melting of the system with a free surface. In such a case the melting, therefore, began at the surface. In the present work, the periodic boundary condition is applied to the system, so that the study is concerned with melting in the bulk, in which the formation of the lattice defect takes place before the melting.

Nosé and Yonezawa [18] studied the melting and crystallization in a Lennard-Jones system by an MD method with the periodic boundary condition and showed that the formation

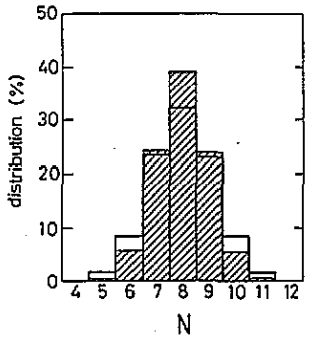

Figure 11. Histograms of the number of neighbour Ag ions around an Se ion in the superionic (fine lines with oblique shading, at 950 K) and molten (bold lines, at 1200 K) states.

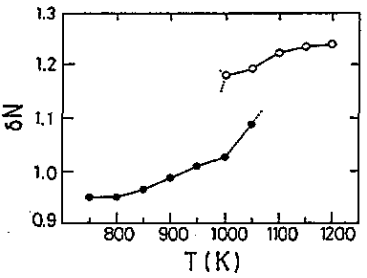

Figure 12. Temperature dependence of the standard deviation in the number of neighbour Ag ions, δN, around an Se ion for heating (filled circles) and cooling (open circles) processes.

of the lattice defect is observed before melting. We have seen that the weakness of the restoring force relative to the short-range force component plays an important role in creating the Se defect. We guess that the defect in the Lennard-Jones system might be created in the same manner. The long-range Coulomb force in ionic crystals makes their cohesive energy larger than that of the Lennard-Jones system, with the result that the melting point in the former is much larger than that in the latter.

4. Summary

By means of a constant-pressure and constant-temperature molecular dynamics simulation, the crystallization and melting of an Se sublattice in the superionic conductor Ag_2Se have been investigated. For the interaction between ions, the effective interionic potential of Rino *et al* has been used. By lowering the temperature of the molten state, Se ions crystallize successfully to a BCC lattice and the superionic (α) state appears. The transition temperature is estimated to be about 1000 K, which is in reasonable agreement with the experimental value of 1170 K. Interstitial defects in the Se sublattice occur in the melting process. By studying the process of defect formation in detail, it becomes obvious that the repulsive force acting on an Se ion from Ag ions behaves as a restoring force maintaining the Se sublattice. It is also observed that the formation of the defect is promoted when marked inhomogeneity in the local density of Ag ions takes place and the restoring force weakens.

References

[1] Rahman A 1976 *J. Chem. Phys.* **65** 4845
[2] Gillan M J and Dixon M 1980 *J. Phys. C: Solid State Phys.* **13** 1901
[3] Dixon M and Gillan M J 1980 *J. Phys. C: Solid State Phys.* **13** 1919
[4] Walker A B, Dixon M and Gillan M J 1982 *J. Phys. C: Solid State Phys.* **15** 4061
[5] Gillan M J 1985 *Physica* B **131** 157
[6] Gillan M J 1986 *J. Phys. C: Solid State Phys.* **19** 3391
[7] Dickens M H, Hayes W, Hutchings M T and Smith C 1980 *Harwell Report* MPD/NBS/153
[8] Wolf M L, Walker J R and Catlow C R A 1984 *J. Phys. C: Solid State Phys.* **17** 6623
[9] Andersen H C 1980 *J. Chem. Phys.* **72** 2384
[10] Parrinello M, Rahman A and Vashishta P 1983 *Phys. Rev. Lett.* **50** 1073

[11] Tallon J 1986 *Phys. Rev. Lett.* **57** 2427
[12] Ray J R and Vashishta P 1989 *J. Chem. Phys.* **90** 6580
[13] Shimojo F and Okazaki H 1991 *J. Phys. Soc. Japan* **60** 3745
[14] Rino J P, Hornos Y M M, Antonio G A, Ebbsjö I, Kalia R K and Vashishta P 1988 *J. Chem. Phys.* **89** 7542
[15] Wiegers G A 1971 *Am. Mineral.* **56** 1882
[16] Jensen E J, Kristensen W D and Cotterill R M J 1973 *Phil. Mag.* **27** 623
[17] Mandell M J, McTague J P and Rahman A 1976 *J. Chem. Phys.* **64** 3699
[18] Nosé S and Yonezawa F 1986 *J. Chem. Phys.* **84** 1803
[19] Tanemura M, Hiwatari Y, Matsuda H, Ogawa T, Ogita N and Ueda A 1977 *Prog. Theor. Phys.* **58** 1079
[20] Tanemura M, Hiwatari Y, Matsuda H, Ogawa T, Ogita N and Ueda A 1978 *Prog. Theor. Phys.* **59** 323
[21] Cape J N, Finney J L and Woodcock L V 1981 *J. Chem. Phys.* **75** 2366
[22] Tanemura M, Matsuda H, Ogawa T, Ogita N and Ueda A 1990 *J. Non-Cryst. Solids* **117/118** 883
[23] Martin C H and Singer S J 1991 *Phys. Rev.* B **44** 477
[24] Amini M, Fincham D and Hockney R W 1979 *J. Phys. C: Solid State Phys.* **12** 4707
[25] Nosé S 1984 *Mol. Phys.* **52** 255
[26] Nosé S 1986 *Mol. Phys.* **57** 187
[27] Nosé S 1984 *J. Chem. Phys.* **81** 511
[28] Gear G W 1971 *Numerical Initial Value Problems in Ordinary Differential Equations* (Englewood Cliffs, NJ: Prentice Hall) ch 9
[29] Finney J L 1979 *J. Comput. Phys.* **32** 137
[30] Tanemura M, Ogawa T and Ogita N 1983 *J. Comput. Phys.* **51** 191
[31] Hsu C S and Rahman A 1979 *J. Chem. Phys.* **70** 5234
[32] Tanaka M 1986 *J. Phys. Soc. Japan* **55** 3108
[33] Okazaki H 1967 *J. Phys. Soc. Japan* **23** 355
[34] Kagakukai N (ed) 1984 *Kagakubinran* (Tokyo: Maruzen) (in Japanese)